KSME Journal, Vol. 7, No. 3, pp. 194~202, 1993

Residual Stress Analysis of an External Grooved Thick-Walled Pressure Vessel

Seung-Kee Koh*

(*Received July 24, 1992*)

Residual stress analysis of an autofrettaged thick-walled pressure vessel containing an external groove was described in order to calculate the stress concentration at the external groove. The autofrettage residual stress distributions of the external grooved thick-walled pressure vessel were simulated using an equivalent thermal loading from the analogy of thermal and autofrettage residual stress fields. Thermal stresses due to the simulated thermal loadings for various degrees of autofrettage overstrain level were computed using finite element methods. Very high stress concentration factors due to autofrettage loadings were obtained at the external groove root that contained a sharp root radius. Experimental measurement of residual stresses for a fully autofrettaged smooth thick-walled pressure vessel using an equivalent saw cut method resulted in very close agreement with the theoretical autofrettage residual stress distributions. The stress analysis results implied that the autofrettage residual stress concentration might cause a cracking problem at the external groove root of the thick-walled pressure vessel, indicating that lower autofrettage overstrain and a groove geometry change were desirable for enhanced durability.

Key Words: Residual Stress, Autofrettage, Overstrain, Thermal Loading Analogy, Equivalent Saw Cut

Nomenclature

a : Inside radius of pressure vessel
b : Outside radius of pressure vessel
d : Depth of external groove
E : Young's modulus
h : Width of external groove
K_t : Theoretical stress concentration factor
M : Bending moment
$O.S.$: Overstrain
R : Radius of curvature at external groove root
T_a : Temperature at $r=a$
T_ρ : Temperature at $r=\rho$
W : Thickness of pressure vessel ($=b-a$)
ρ : Elastic-plastic radius of the autofrettaged pressure vessel
ν : Poisson's ratio
γ : Split opening angle
σ_N : Nominal stress
σ_{max} : Maximum stress
σ_r : Radial stress
σ_θ : Tangential stress
σ_z : Longitudinal stress
σ_{ys} : Yield strength

* Mechanical and Production Engineering Dept. Kunsan National University, Kunsan, Chonbuk 573-360, Korea

1. Introduction

If a sufficiently high internal pressure is applied to a cylindrical thick-walled pressure vessel, plastic deformation will begin at the inside diameter and extend through the cylinder wall as the pressure is increased. Due to nonuniform elastic recovery after release of the internal pressure, the outer portion of the cylinder attempts to resume its original size, but the inner portion of the

cylinder, which was deformed a greater amount, tries to remain permanently deformed. This process results in a compressive tangental residual stress near the inside diameter that varies logarithmically to tension through the plastically deformed region of the cylinder. The process of producing residual stresses by means of plastic deformation of the pressure vessel is known as autofrettage (Franklin, 1960).

Compressive tangential residual stresses at the inside diameter due to the autofrettage process increase the strength and retard fatigue crack formation and growth at the pressure vessel under the pulsating internal pressure loading. It has been shown that autofrettage significantly increases the fatigue life of internally pressurized thick-walled pressure vessels in which fatigue failures originate at the inside surface (Morrison, 1969; Davidson, 1963; Kapp, 1982). However, the tangential tensile residual stresses at the outside surface are of great concern when discontinuities such as grooves and keyways are introduced at the outside diameter. These external structural discontinuities cause a redistribution of the autofrettage residual stresses along with high stress concentrations at the discontinuities and have resulted in fatigue failures of pressure vessels (Pu, 1981). In order to estimate fatigue failures of the pressure vessels, therefore, it is very important to analyze the residual stress distribution of the autofrettaged thick-walled pressure vessel when the pressure vessel contains a groove at the outside diameter.

In this paper, analytical residual stress distributions of an autofrettaged thick-walled pressure vessel which contains a groove at the outside diameter were obtained in order to determine the residual stress concentration at the external groove. This groove is used for a keyway which is necessary for the pressure vessel design. Autofrettage residual stress distributions for 50, 75, and 100 percent overstrain, where percent overstrain is defined as the percentage of wall thickness subjected to plastic deformation during the application of autofrettage pressure, were simulated using a thermal loading analogy and finite element methods. For the case of fully autofrettaged smooth thick-walled pressure vessel, residual stresses were measured experimentally using an equivalent cut method and compared to theoretical solution.

2. Residual Stress Distributions of an Autofrettaged Smooth Thick-Walled Pressure Vessel

Theoretical stress distributions of a partially autofrettaged smooth thick-walled pressure vessel based on the assumptions of the Tresca yield criterion, elastic-perfectly plastic material behavior, plane strain conditions, and no reverse yielding nor Bauschinger effect are given as (Davidson, 1963),

$$\sigma_r=\sigma_{ys}\left\{\frac{a^2}{b^2-a^2}\left(1-\frac{b^2}{r^2}\right)\left[\frac{\rho^2-b^2}{2b^2}-\ln\frac{\rho}{a}\right]+\left[\frac{\rho^2-b^2}{2b^2}-\ln\frac{\rho}{r}\right]\right\} \quad \text{for } a\le r\le\rho$$

$$\sigma_{ys}\left(1-\frac{b^2}{r^2}\right)\left\{\frac{\rho^2}{2b^2}+\frac{a^2}{b^2-a^2}\left[\frac{\rho^2-b^2}{2b^2}-\ln\frac{\rho}{a}\right]\right\} \quad \text{for } \rho\le r\le b \tag{1a}$$

$$\sigma_\theta=\sigma_{ys}\left\{\frac{a^2}{b^2-a^2}\left(1+\frac{b^2}{r^2}\right)\left[\frac{\rho^2-b^2}{2b^2}-\ln\frac{\rho}{a}\right]+\left[\frac{\rho^2+b^2}{2b^2}-\ln\frac{\rho}{r}\right]\right\} \quad \text{for } a\le r\le\rho$$

$$\sigma_{ys}\left(1+\frac{b^2}{r^2}\right)\left\{\frac{\rho^2}{2b^2}+\frac{a^2}{b^2-a^2}\left[\frac{\rho^2-b^2}{2b^2}-\ln\frac{\rho}{a}\right]\right\} \quad \text{for } \rho\le r\le b \tag{1b}$$

$$\sigma_z=\sigma_{ys}\left\{\frac{\nu(\rho^2-a^2)}{b^2-a^2}-\frac{2\nu a^2}{b^2-a^2}\ln\frac{\rho}{a}-2\ln\frac{\rho}{r}\right\} \quad \text{for } a\le r\le\rho$$

$$\sigma_{ys}\left\{\frac{\nu(\rho^2-a^2)}{b^2-a^2}-\frac{2\nu a^2}{b^2-a^2}\ln\frac{\rho}{a}\right\} \quad \text{for } \rho\le r\le b, \tag{1c}$$

where the radius ρ denotes the radius of the elastic-plastic boundary during the autofrettage process. If von Mises yield criterion were used for the derivation of the autofrettage residual stresses (Morrison, 1960), then the same equations would be obtained, except that $2\sigma_{ys}/\sqrt{3}$ would replace σ_{ys} in Eq. (1).

Theoretical autofrettage residual stresses obtained above by the elastc-plastic analysis also can be determined using an equivalent thermal

loading (Hussain, 1980). If there is a steady state heat flow such that T_a and T_ρ are the temperatures at $r=a$ and $r=\rho$ of the pressure vessel respectively, then the temperature distribution of the smooth pressure vessel becomes

$$T = T_\rho + \frac{(T_a - T_\rho)}{\ln(\rho/a)} \ln\left(\frac{\rho}{r}\right) \quad \text{for } a \le r \le \rho$$
$$= T_\rho \quad \text{for } \rho \le r \le b \tag{2}$$

In this thermal loading, the radius ρ corresponds to the elastic-plastic radius in the elastic-plastic analysis of the autofrettage residual stress distribution. The resulting thermal stress distributions due to thermal loading given in Eq. (2) are the same as those given in Eq. (1), if the yield strength, σ_{ys}, in Eq. (1) is replaced by the following relation,

$$\frac{\alpha E}{2(1-\nu)} \frac{(T_a - T_\rho)}{\ln(\rho/a)} = \sigma_{ys}, \tag{3}$$

where α is the coefficient of thermal expansion. Therefore, if an equivalent temperature given in Eq. (3) were imposed on the thick-walled pressure vessel, thermal stress distributions would be theoretically equal to the autofrettage residual stress distributions.

In Eq. (1) for the autofrettage residual stress distributions, the compressive tangential residual stress occurs at the bore region and varies logarithmically to tension through the wall. Therefore, radial cutting through the thickness of an autofrettaged pressure vessel causes an opening of the pressure vessel due to a relaxation of the residual stresses analogous to the form of a pure bending moment. The theoretical residual stresses for a 100 percent overstrain can be obtained by solving an elastic problem of a curved beam subjected to a pure bending moment, M, necessary to join the split opening angle, γ, as shown in Fig. 1, resulting in (Timoshenko, 1970),

$$\sigma_r = \frac{\gamma E}{4\pi}\left[-\ln\frac{b}{r} - \frac{a^2}{b^2-a^2}\left(1-\frac{b^2}{r^2}\right)\ln\frac{b}{a}\right]$$
$$\sigma_\theta = \frac{\gamma E}{4\pi}\left[1-\ln\frac{b}{r} - \frac{a^2}{b^2-a^2}\left(1+\frac{b^2}{r^2}\right)\ln\frac{b}{a}\right] \tag{4}$$

Similarity between Eq. (4) and the theoretical residual stresses for a 100 percent overstrian, i.e., $\rho=b$ in Eq. (1) yields

$$\frac{\gamma E}{4\pi} = \sigma_{ys} \text{ or } \frac{\sqrt{3}\gamma E}{8\pi} = \sigma_{ys}, \tag{5}$$

depending on the Tresca or von Mises yield criteria assumed in the elastic-plastic stress analysis, respectively.

In order to experimentally determine the autofrettage residual stresses for a 100 percent overstrain case using the equivalent saw cutting method, rings of 20 mm thickness were taken from a fully autofrettaged smooth thick-walled pressure vessel and were saw-cut through the thickness as shown in Fig. 2. Theoretical stress distributions in the thick-walled pressure vessel due to 100 percent overstrain are equivalent to the stress distributions in a curved beam due to the bending moment which is required to put the split ring together. Therefore, if an autofrettaged ring were cut through the thickness, then the cut would

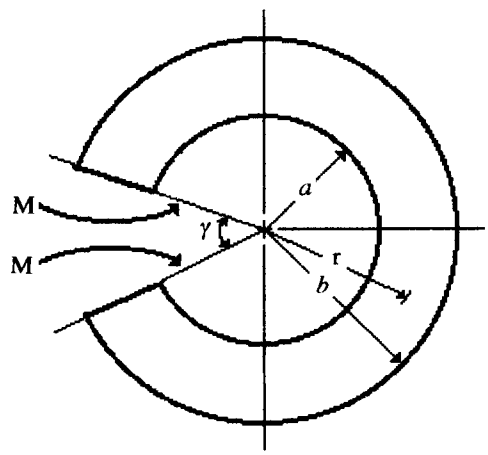

Fig. 1 Curved beam subjected to pure bending moment

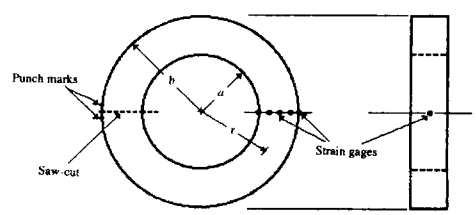

Fig. 2 Saw-cut of autofrettaged ring and strain gage locations

make a certain opening angle of the split ring due to the relaxation of the tangential autofrettage residual stresses. As shown in Fig. 2, punch marks were made to measure the split opening angle and a series of strain gages were attached on the opposite side surface of the saw-cut. Combinations of uniaxial and 45 degree rosettes were used across the thickness of the wall.

3. Residual Stress Distributions of an Autofrettaged Thick-Walled Pressure Vessel with an External Groove

In many practical cases, external discontinuities such as keyway grooves, holes, and cracks can be present in a thick-walled pressure vessel. These discontinuities cause a redistribution of residual stresses that may be difficult to determine using elastic-plastic analysis. In this paper, autofrettage residual stresses in a thick-walled pressure vessel with an external groove were found using a finite element method and thermal loading analogy.

Linear elastic stress analysis of a thick-walled pressure vessel with an external groove using the finite element method was performed. The vessel was subjected to thermal loading for the simulation of autofrettage. Configuration of the pressure vessel with a rectangular groove at the outside surface is shown in Fig. 3, where plane A-A′ is the radial plane opposite to the external groove, and planes B-B′ and C-C′ are ther radial planes through the groove root and the center of the groove, respectively. The pressure vessel has an inside radius, a, of 85 mm and outside radius, b, of 142 mm. Wall thickness ratio, defined as b/a, is 1.67. Groove root radius, R, is 1.5 mm. Three autofrettage loading conditions 100, 75, and 50 percent overstrain, were analyzed. In the thermal loading analogy, the equivalent temperature distribution given by Eq. (3) was imposed, depending on percent overstrain conditions.

Due to the symmetry of the pressure vessel, as shown in Fig. 3, only half of a segment of the pressure vessel was used for the finite element analysis. The ANSYS finite element program was employed to perform the analysis (Desalvo, 1985). A typical finite element mesh used to find solutions is shown in Fig. 4. Boundary conditions are shown in Fig. 4(a) and a refined mesh near the groove root is shown in Fig. 4(b). For thermal loading, the temperature distribution due to steady state heat flow was first analyzed using the

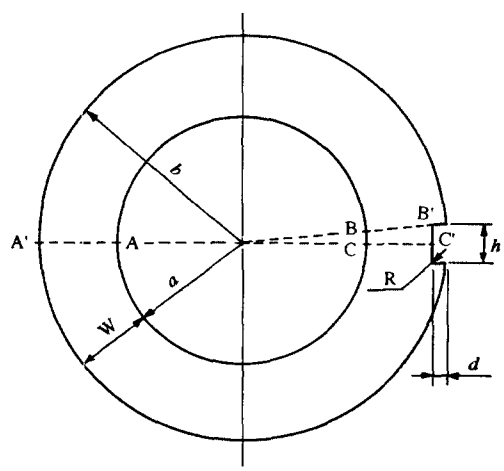

Fig. 3 Thick-walled pressure vessel with an external groove ($a=85$, $b=142$, $d=10$, $h=25$, $W=57$, $R=1.5$, unit : mm)

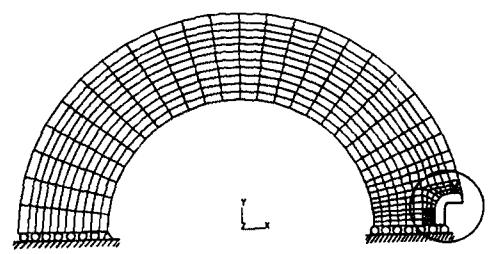

(a) Generated mesh

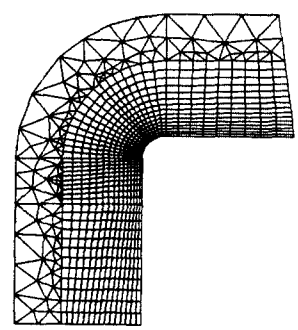

(b) Refined mesh near the root of groove

Fig. 4 Finite element mesh used for stress analysis

finite element program, and then the nodal temperature results were transferred as an input for the thermal stress calculations. Plane strain conditions with $\varepsilon_z=0$, where z is the longitudinal direction, was used for all loading cases in the analysis of the thick-walled pressure vessel.

For the finite element modeling, three different types of two dimensional plane strain solid elements were used : a 4 node isoparametric quadrilateral element, a 6 node isoparametric triangular element, and an 8 node isoparametric quadrilateral element. For each element type, convergence was checked in order to ensure correct results avoiding possible input errors and inherent errors in some element types. In the final meshes, the number of elements around one quarter of the groove root circle for the 4 node quadrilateral element, 6 node triangular element, and 8 node quadrilateral element were 28, 20, and 12, resulting in element sizes of 0.06, 0.12, and 0.15 mm, respectively.

4. Results and Discussion

In order to determine the autofrettage residual stresses using the thermal loading analogy, a temperature distribution due to the steady state heat flow must be found. The initial temperature input for the steady state heat flow was calculated from the Eq. (3) using the yield strength, σ_{ys}, of 1170 MPa, Young's modulus, E, of 210 GPa, thermal expansion coefficient, α, of 6.8×10^{-6}/℃, and Poisson's ratio of 0.29. The initial temperature, T_a, at the inside radius $r=a$ resulted in 589, 467, and 332℃ for 100, 75, and 50 percent overstrain cases, respectively. Since the thermal stresses result from the temperature gradient, the temperature, T_ρ, at the radius $r=\rho$ was assigned as zero for convenience. After performing the temperature analysis using the ANSYS program, the finite element analysis was again performed to obtain the thermal stresses from the computed nodal temperature. These thermal stresses are equivalent to the autofrettage residual stresses as already mentioned.

Finite element stress distributions for each overstrain condition along the planes A-A′, B-B′, and C-C′, denoted in Fig. 3, are shown in Figs. 5 to 7, where the data points represent the finite element solutions and the solid lines represent the interpolation curves of the finite element solutions. A very high stress concentration at the groove root can be clearly noticed for each autofrettage loading case. Finite element solutions of the tangential residual stresses along plane A-A′ for each overstrain level resulted in very close agreement with the theoretical solutions in Eq. (1b) derived for the smooth thick-walled pressure vessel, implying the negligible influence on the stress distribution by the existence of an external groove. The differences between these finite ele-

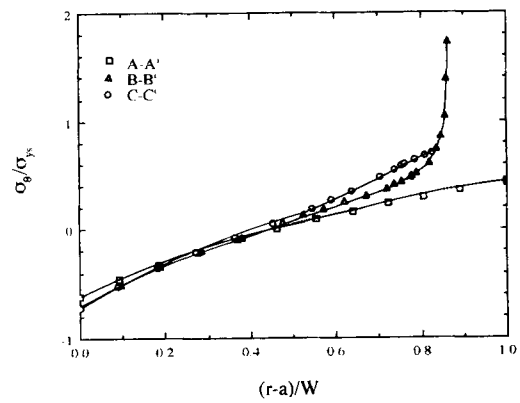

Fig. 5 Tangential stress distributions due to 100 percent overstrain loading along A- A′, B-B′, and C-C′ in a thick-walled pressure vessel

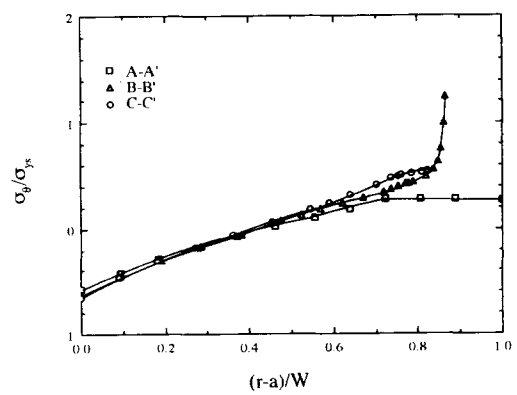

Fig. 6 Tangential stress distributions due to 75 percent overstrain loading along A-A′, B-B′, and C-C′ in a thick-walled pressure vessel

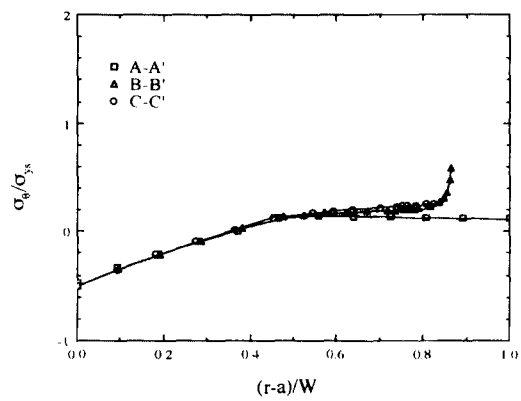

Fig. 7 Tangential stress distributions due to 50 percent overstrain loading along A-A′, B-B′, and C-C′ in a thick-walled pressure vessel

ment solutions and the theoretical solutions were less than 3 percent.

The theoretical stress concentration factor, K_t, defined as

$$K_t = \frac{\sigma_{\max}}{\sigma_N}, \tag{6}$$

was calculated at both the root and the center of the groove. Nominal stress, σ_N, was defined as the stress occurring at the outside radius for the reduced wall thickness. From Eq. (1b), using a reduced thickness, the tangential stress at the outside radius, i, e., $r = b_0 = b - d$, was defined as the nominal stress by

$$\sigma_N = \sigma_{ys}\left\{\frac{\rho^2}{b_o^2} + \frac{2a^2}{b_o^2 - a^2}\left[\frac{\rho^2 - b_o^2}{2b_o^2} - \ln\frac{\rho}{a}\right]\right\} \tag{7}$$

As shown in Figs. 5 to 7, the magnitude of compressive tangential residual stress at the inside radius increases as the percent overstrain increases. This implies that for both yielding and fatigue problems, a higher internal operating pressure can be applied to a smooth thick-walled pressure vessel that has been subjected to a larger overstrain. It was reported that a 100 percent overstrain condition resulted in the maximum fatigue life for a smooth thick-walled pressure vessel without any external grooves, where cracks grew from the inside surface (Davidson, 1963). However, it can be observed that the maximum tensile stress at the external groove root increases as the percent overstrain increases, meaning that longer fatigue crack formation and growth life at the external groove root will occur for a small percent overstrain under the same pulsating internal pressure.

Maximum principal stresses, $\sigma_{\max}$, at the locations B′ and C′, as shown in Fig. 3, along with the nominal stress, σ_N, and stress concentration factors are shown in Table 1 for each overstrain loading case. Significant differences in the maximum principal stresses for different percent overstrain are shown in Table 1. At the groove root, i. e., location B′, the maximum principal stress in a 100 percent overstrain case was 40 and 195 percent higher than in 75 and 50 percent overstrain cases, respectively. However, essentially no differences in K_t between 75 and 50 percent overstrain cases for both the center and root of the groove can be seen in Table 1. Also, theoretical stress concentration factors at points B′, and C′ for 100 percent case were only 16 and 8 percent higher than for 75 percent and 50 percent overstrain cases, respectively. The small differences in K_t, compared to the large differences in the maximum principal stress between percent overstrain cases at both center and the root of the

Table 1 Nominal stresses, finite element solutions of maximum principal stresses and theoretical stress concentration factors for autofrettage loading

Loading condition		$\sigma_{\max}$ @ B′ (MPa)	$\sigma_{\max}$ @ C′ (MPa)	σ_N (MPa)	K_t	
					@ B′	@ C′
Percent	100	2044	825	440	4.65	1.88
Overstrain	75	1462	633	368	3.97	1.72
	50	692	299	170	4.07	1.76

groove were due to the similar difference in the ratio between maximum and nominal stresses.

Maximum principal stress contour plot near the groove root due to 100 percent overstrain loading is shown in Fig. 8, where θ is an angle measured from the beginning of the curvature along the contour of the external groove root. Similar stress contours near the groove root due to 75 and 50 percent overstrain loadings were obtained. Maximum principal stress contours from all loading conditions showed significant stress concentration at the sharp root of the groove. Figure 9 shows the maximum principal stresses along the groove root surface. Regardless of the loading conditions, the peaks of maximum principal stress occurred at the angle θ between 15 to 20 degree, denoted in Fig. 8, from the beginning of the root curvature, and they decreased very rapidly as the angle increased.

Figure 10 shows the autofrettage residual stress distributions calculated from the relaxed strains by the saw-cut across the thickness of the wall. The data points represent the experimental stress values with opposite signs after the saw-cut, while the lines represent the theoretical residual stress values prior to saw-cut. The tangential relaxation stress data, calculated from the uniaxial strain gages using $\sigma = E\varepsilon$, were expected to be in error, which turned out to be small compared to the calculated relaxed stress data from the rosettes using generalized Hooke's law, as shown in Fig. 10. This was attributed to the relatively small magnitude of radial relaxation stress. Good agreement of the residual stress distributions between the experimental measurements and theoretical calculations can be seen in Fig. 10, especially for von Mises criterion. Noticeable scatter in the tangential residual stress distributions between

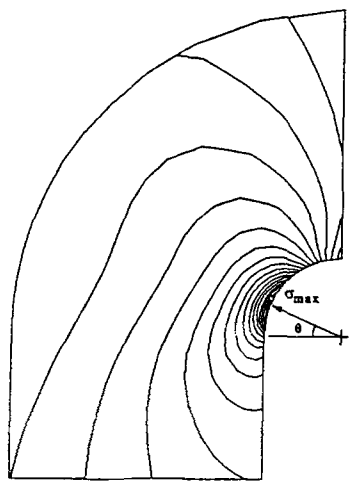

Fig. 8 Maximum principal stress contours near the groove root due to 100 percent overstrain loading

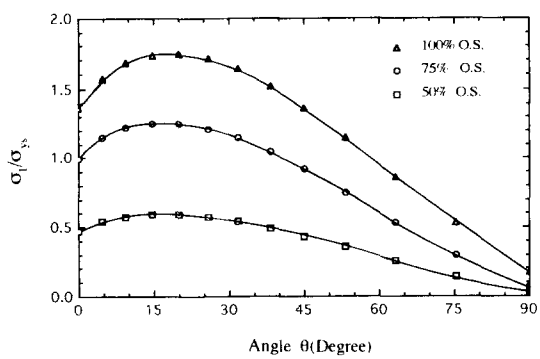

Fig. 9 Maximum principal stress variations along the groove root due to each loading condition

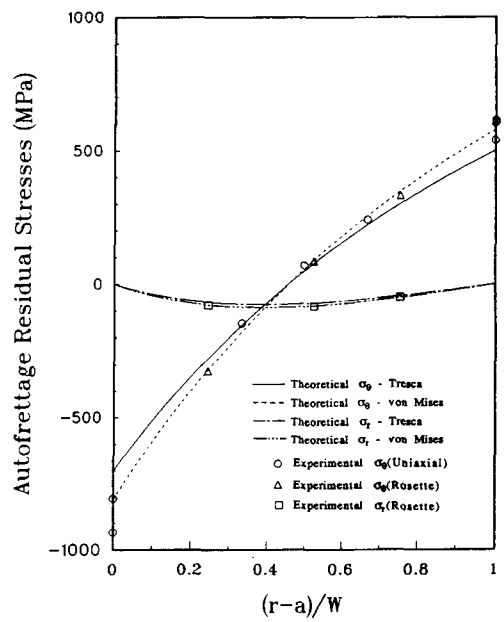

Fig. 10 Autofrettage residual stress distributions across the thickness for a 100 percent thick-walled pressure vessel

Table 2 Split opening angles from the saw-cut of autofrettaged rings

Experimental opening angle (Degree)*	Theoretical opening angle (Degree)
4.98, 4.97, 4.68, 5.05	4.21 (Tresca)
4.84, 5.04, 5.25	4.86 (von Mises)

* Average value : 4.97

experiment and theory can be seen at both the inside and outside surfaces. This was attributed to the assumptions made on the theoretical derivation regarding elastic-perfectly plastic material behavior and yield criteria. The maximum difference in tangential residual stress between experimental and theory was observed at the bore, resulting in approximately 28 percent for the Tresca criterion and 9 percent for the von Mises criterion.

The distance between the punch marks measured after the saw-cut was used for split angle calculations. The opening angles obtained from the seven rings taken from the autofrettaged pressure vessel are listed in Table 2 along with the average angle. These values can be compared to the theoretical opening angles calcuated from Eq. (5). The experimental opening angle showed closer results to the theoretical opening angle based on the von Mises yield criterion than the Tresca yield criterion.

5. Conclusions

(1) Autofrettage residual stresses were determined by imposing an equivalent thermal loading to an external grooved thick-walled pressure vessel. Finite element solutions of tangential stresses along the thickness opposite to the external groove were not influenced by the existence of an external groove, resulting in excellent agreement between the finite element solutions and theoretical solutions.

(2) Experimental measurements of the autofrettage residual stresses using both split opening angles and relaxed strains due to the saw-cut of a fully autofrettaged smooth pressure vessel showed very close agreemet with the theoretical solutions.

(3) Significantly high theoretical stress concentration factors, K_t, of 4.65, 3.97 and 4.07 were obtained at the external groove root due to 100, 75 and 50 percent overstrain loadings, respectively, from the finite element analysis. Peaks of the maximum principal stresses regardless of loading conditions occurred at an angle between 15 and 20 degrees from the beginning of the root curvature, which was considered as the most vulnerable location for pressure vessel failure.

(4) The stress analysis results showed a high possibility of failure at the groove root due to the high stress concentration. This indicates that the failure can be avoided or the life of the pressure vessel can be extended by changing the groove shape to alleviate the stress concentration at the root, and by decreasing the percent overstrain to a certain optimum level in order to reduce the tensile tangential residual stresses at the outside diameter without sacrificing the beneficial compressive tangential residual stresses at the bore.

Acknowledgements

This paper was supported by non directed research fund, Korea Reseach Foundation, 1992.

References

Davidson, T.E., Eisenstadt, R. and Reiner, A. N., 1963, "Fatigue Characteristic of Open-End Thick-Walled Cylinders Under Cyclic Internal Pressure," Journal of Basic Engineering, Trans. ASME, pp. 555~565.

Davidson, T.E. and Kendall, D.P., 1970, "Design of High Pressure Containers and Associated Equipments," *The Mechanical Behavior of Materials under Pressure,* Pugh, H.Ll.D., Editor, Elsevier Publishing, Amsterdam, pp. 54~118.

Desalvo, G. and Swanson, J.A., 1985, ANSYS User's Manual, Swanson Analysis System, Inc.

Franklin, G.J. and Morrison, J.L.M, 1960, "Autofrettage of Cylinders : Prediction of Pressure/External Expansion Curves and Calculation of Residual Stresses," Proceedings of Institution

of Mechanical Engineers, Vol. 174, No. 35, pp. 947~974.

Hill, R., 1950, *The Mathematical Theory of Plasticity,* Oxford University Press, London.

Hussain, M.A., Pu, S.L., Vasilakis, J.D. and O' Hara, P., 1980, "Simulation of Partial Autofrettage by Thermal Loads," ASME Journal of Pressure Vessel Technology, Vol. 102, pp. 314~318.

Kapp, J.A. and Pu, S.L., 1982, "Fatigue Design of Thick-Walled Cylinder Considering the OD as a Failure Site," Pressure Vessel Design, PVP-57, American Society of Mechanical Engineers.

Morrison, J.L.M., Crossland, B. and Parry, J.C. S, 1960, "Strength of Thick-Walled Cylinders Subjected to Repeated Internal Pressure," Journal of Engineering for Industry, Trans. ASME, pp. 143~153.

Pu, S.L. and Hussain, M.A., 1981, "Residual Stress Redistribution Caused by Notches and Cracks in Partially Autofrettaged Tube," ASME Journal of Pressure Vessel Technology, Vol. 103, pp. 302~306.

Timoshenko, S.P. and Goodier, J.N., 1970 *Theory of Elasticity,* McGraw-Hill, New York.